

Daniel A. Hipp

Photocurrent Sampling in free Air

Bachelor Thesis

to achieve the university degree of Bachelor of Science Bachelor's degree programme: Physik

submitted to

Graz University of Technology

Supervisor Univ.-Prof. Dipl.-Phys. Dr.rer.nat.habil. Martin Schultze Institute of Experimental Physics

Graz, June 2023

Affidavit

I declare that I have authored this thesis	independently, that I have not used other than
the declared sources/resources, and that	I have explicitly indicated all material which
has been quoted either literally or by con	tent from the sources used. The text document
uploaded to TUGRAZonline is identical to	the present bachelor thesis.
Date	Daniel Alexander Hipp

Acknowledgments

I would like to express my gratitude to several individuals who have played a significant role in my journey towards completing my bachelors degree. Their guidance, support and encouragement have been invaluable.

First and foremost, I am grateful to my supervising professor, Martin Schultze, for providing me the possibility to perform my own experiment on such a interesting topic and his support and guidance throughout my research. Thanks to Marcus Ossiander for sharing his technical expertise in the lab and shaping my understanding of the subject matter. I would also like to extend my heartfelt appreciation to Olga Resel for providing me insight into the mechanisms of autocorrelation and guidance for the structure of this thesis. Furthermore, I would like to acknowledge my friend Jan Priedigkeit for those intriguing discussions, inspiration and support throughout my academic journey. Without him I would never be able to finish my bachelors degree. Finally, I would like to thank my parents for their believe in my abilities and their support throughout my studies

Abstract

Time resolved measurements in the femtosecond regime can be realized by pump probe experiments with ultrashort laser pulses. By measuring an observable that is modulated with the pump probe delay we gain access to ultrafast processes down to the timescale of the laser pulse duration. Such modulated quantities are typically intensity, polarization, spectral composition or frequency modulation, however also photocurrents are suitable. The possibility of measuring photocurrents, stemming from ionization of air by high intensity femtosecond laser pulses, is investigated in this thesis. To measure the currents in the picoampere (pA) range, an amplifier based on an operational amplifier in transimpedance amplifier configuration is developed. The pump probe experiment yields autocorrelation data of the laser pulse, as well as an infrared spectral response of the air. By enhancing the signal to noise ratio and resolution, we will be able to identify molecular energy levels within the signal.

Contents

1	Intro	oduction		6
2	Amı	olifier Des	sign	6
	2.1		ments	. 6
	2.2	Amplific	eation Method	. 7
		2.2.1 J	FETS	. 7
		2.2.2 D	Oarlington Transistors	. 8
		2.2.3 C	Op Amps as non inverting Amplifier	. 8
		2.2.4 C	Op Amps as Transimpedance Amplifier	. 8
	2.3	Final Cir	rcuit Design	. 9
			Noise and Bandwidth	
		2.3.2 P	Power Supply and Ground	. 11
			Temperature Control	
		2.3.4 P	PCB Layout	. 12
		2.3.5 F	Further Improvements	. 13
	2.4	Verificat	ion	. 14
3	Exp	erimental	Setup	17
	3.1	Electrica	al Setup	. 17
	3.2		Setup	
	3.3		ng a Single Pulse	
	3.4		ace Measurement	
		3.4.1 S	Signal Acquisition	. 20
		3.4.2 S	Signal Distortion	. 20
4	Resi	ılts		21
5	Disc	ussion		24
6	Con	clusion		26

1 Introduction

Ultrashort laser pulses are the ultimate tool to research fast physical and chemical processes in the time domain. Time resolution in experiments exploring dynamical processes is dictated by the pulse length, therefore femtosecond resolution can be achieved with modern laser systems. Such experiments utilize a pump probe design, in which one pulse is delayed with regard to another one and only the difference in arrival time is relevant for the outcome. Delaying a pulse can be done on a fine scale by lengthening the optical path. At a specific delay time, a constant signal is produced by the interaction of the two pulses. In other words, time can be "frozen" at any desired delay time, thus enabling measurement techniques that are slow, compared to optical time scales, to acquire information on ultrafast processes.

In this thesis, the signal is a photocurrent, stemming from ionized molecules in the lasers path. The current is captured by two conductive plates above and below the focus, similar to a capacitor arrangement. The energy of a single photon at the lasers wavelength is not enough to ionize any molecule in the air, but by focusing the beam to a small area, high intensities are reached that allow for multi photon processes to happen. Because multi photon ionization is a nonlinear interaction, the amount of ions is dependent on the delay time of the pulses. It reaches its maximum at zero delay, when the overlapping pulses interfere constructively to produce the highest field strength, thereby increasing ionization efficiency. In essence, the pulse can be probed with itself. This is desirable since it is hard to find another signal, short enough to probe the pulse, while being coherent with it.

This thesis is split into two main parts, the design and construction of an amplifier enabling the measurement of photocurrents in chapter 2 and the actual measurement of a timetrace in a pump probe experiment in free air. While scientific instruments to amplify photocurrents are available, it is chosen to leverage the possibility of modern consumer electronics to build a low cost amplifier optimized for this specific task. Although the current signal from photoionization is unknown at the design stage, some assumptions can be made on which the desired properties of the amplifier are based. This process included some guessing, but the choices made were ultimately justified by the success of the experiment.

2 Amplifier Design

2.1 Requirements

In order to start designing a circuit for signal detection, the nature of the signal has to be known. The signal quality can be divided into temporal properties and electrical properties.

As the laser pulses of a mode locked laser are very short (in the order of fs), those will not be temporally resolved. Instead the goal is to resolve individual pulses, which are separated by $\frac{1}{f_{ren}}$. This translates to the condition that the bandwidth of the

amplifier f_{-3dB} should be bigger than the repetition rate of the laser f_{rep} .

As for the electrical characteristics, a current consisting of the ionised particles and / or electrons is expected, rather than a voltage signal. In order to not repel the charged particles, the receiving electrode should remain at a constant potential, meaning the burden voltage at the input shall be minimal. It may be necessary to apply a voltage bias with a second electrode, to facilitate directional movement of the charged particles.

To estimate the current, the amount of charges per pulse is multiplied with the repetition rate of the laser. Assuming one elementary charge per pulse at 80 MHz, this yields a current of around 12 pA. The f_{rep} of 80 MHz is the normal operating frequency of the laser intended to be used for the experiment.

Other central qualities of the amplifier are the properties of the output signal. For the estimated input current of 12 pA the output voltage should be at least in the mV range and should be above the noise floor. The amplifier should also be able to drive the signal into an RG58 cable attached to a 1 M Ω oscilloscope input.

2.2 Amplification Method

The expected current of about 10 pA is in the same order of magnitude as currents induced into a cable by external fields or via leakage currents through the isolation. A solution to this problem is to amplify the signal very close to its origin. Because it could be necessary to perform the measurement under vacuum conditions, the amplifier should also be able to withstand those. From the expected input current of 10 pA and the expected output in the tens of mV, a required transimpedance of $> 1~\rm G\Omega$ is deduced.

Different amplification methods were considered in order to fulfill these requirements:

- Junction-gate field-effect transistors (JFETs)
- Darlington transistors
- Op amp as noninverting amplifier
- Op amp as transimpedance amplifier (TIA)

2.2.1 JFETS

Junction-gate field-effect transistors (JFETs) feature a very high input resistance in the order of teraohm (example 2N4117 2 $\mathrm{T}\Omega$, 0.25 pA leakage current [3]). This in combination with their voltage driven switching characteristics, leads to a high current gain if sufficient drain source voltage is applied. Amplifier input stages made from JFETs are employed in electrometers (like in the Keithley 480) and in proportional counters to amplify tiny currents. However those devices feature sophisticated circuits to compensate for unwanted properties of this simple component. Effects of temperature and the formation of a burden voltage, because of the voltage-controlled nature of JFETs, are the most prevalent problems. The complexity of designing such a circuit exceeds the authors capabilities, as well as the scope of this thesis, as the focus shall remain on photocurrent measurement.

2.2.2 Darlington Transistors

Darlington transistors have been successfully used in proportional counters to amplify the tiny current from ionized molecules. They feature high current gains in a single component, typically about $10^4 - 10^5$. The current gain will typically vary a little with the operating point, but linearity is good enough for the intended application. Only at low currents of a few pA or less do we see a breakdown of this behaviour because leakage currents and minority charge carriers begin to play a vital role. As this operating range is far from typical no reliable manufacturer data is available.

Another drawback is that a base emitter voltage about double that of a typical bipolar junction transistor is needed before it starts conducting, which in turn creates a burden voltage on the input. Although this voltage is smaller than on a JFET, additional circuitry is required in order to compensate these effects.

2.2.3 Op Amps as non inverting Amplifier

Non inverting amplifiers can be used in conjunction with a shunt resistor to measure currents and convert them to voltage. This works as long as the shunt current is significantly lower than the input current of the operational amplifier. This is possible due to the high impedance of the non inverting configuration. However, the shunt resistance is also the input resistance of this amplifier, which is therefore relatively high. Depending on the actual shunt resistance and the current, this could lead to a so called burden voltage on the input electrode that is high enough to repel charge carriers. Another undesirable side effect is the bandwidth limit created by the RC-lowpass of input capacitance and shunt resistance. A popular example of such a circuit relevant for photocurrentsampling is the μ CurrentTM GOLD by David L. Jones, which is intended to be used as a precision current adapter for multimeters. It is optimized for low burden voltage and high bandwidth. Jones claims it has a f_{-3dB} of 300 kHz at a maximum transimpedance of 1 M Ω with a minimum resolvable current of 10 pA and a burden voltage of 10 μV per nA [7]. While these parameters seem promising, simulation of the circuit reveals that the noise figures are worse than that of a equivalent transimpedance amplifier, unless a very high shunt resistance (> 100 M Ω) is employed.

2.2.4 Op Amps as Transimpedance Amplifier

A transimpedance amplifier (TIA) fits the description of the task very well, as it linearly converts current into voltage, while keeping the input at a constant potential. Precision of the input is limited by the input bias current and input offset current of the op amp. The bandwidth is defined by the Gain-Bandwidth-Product (GBW) of the op amp, the gain and the parasitic capacitance involved. There are different op amps available which are specifically designed for a similar purpose to the one described in this thesis (e.g. ADA4530-1 from Analog devices, LTC6268 from Linear Technology and LMP7721 from Texas Instruments). This category of op amps is typically called electrometer op amp. Some of those feature input bias currents well below 1 pA.

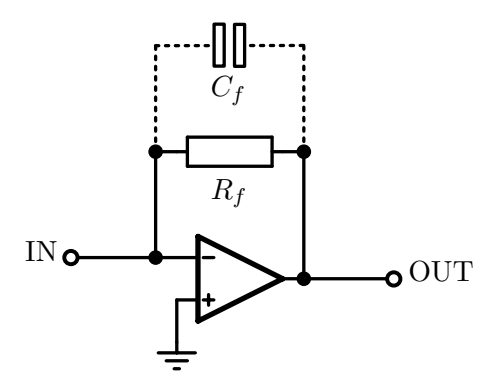


Figure 1: Operational Amplifier in a transimpedance amplifier configuration. The gain of the circuit is defined by the value of the feedback resistor R_f . The feedback capacitance C_f which is composed of parasitic capacitance and / or intentionally added capacitance to limit bandwidth is shown with dotted connections.

2.3 Final Circuit Design

The available data and the ease of use point to a TIA configuration of a low input bias current op amp like the LTC6268-10, as a safe option to achieve the desired amplification with tolerable noise and a reasonable bandwidth.

The LTC6268-10 was chosen because of its extrordinary high GBW of 4 GHz, its low input current of < 60 fA (bias- plus offsetcurrent) and its low input capacitance of only 0.45 pF [12]

2.3.1 Noise and Bandwidth

The goal for the transimpedance was set to 3.3 G Ω . This determines the feedback resistance of the TIA to be at the same value. Unfortunately, the feedback resistance, together with some parasitic capacitance (shown in Figure 1) does also determine the bandwidth according to:

$$f_{-3dB} \approx \frac{1}{2\pi R_f C_f} [5] \tag{1}$$

A possible solution to this is a reduction of the feedback resistor value by some factor B and the addition of another op amp to amplify the output of the TIA by the factor B. This also amplifies the offset voltage of the TIA by the factor B and adds the offset voltage of the second amplifier stage. Reducing the feedback resistor of the TIA has also impacts the Signal-to-Noise Ratio (SNR), because the resistor noise is reduced proportional to the square root of the resistor value B. The RMS noise of a resistor is primarily Nyquist-noise and depends only on the resistor value B, the temperature and the bandwidth D over which the noise is measured [10]:

$$U_{RMSnoise} = \sqrt{4k_B T R \Delta f} \tag{2}$$

Simulation shows, that R_f is the dominant source of noise in the circuit and therefore noise is proportional to $\sqrt{R_f}$.

However, the amplification of the signal is directly proportional to the feedback resistor value R_f and therefore SNR degrades with smaller R_f .

$$SNR = \frac{I_0 R_f}{\sqrt{4k_B T R_f \Delta f}} \propto \sqrt{R_f}$$
 (3)

To summarize, smaller R_f decrease SNR but increases bandwidth. Additional amplification is needed if R_f is less than 3.3 G Ω , but this is limited due to amplification of offset voltage and other signal errors.

By simulating the circuit with LTSpice[©] XVII, a suitable compromise of bandwidth and SNR was found with $R_f = 100 \text{ M}\Omega$

This results in the need for a second amplifier with a gain of 33. To avoid electromagnetic interference and parasitic capacitance on the output of the TIA, this amplifier should be placed as close as possible to the TIA. The obvious choice is another op amp on the same PCB, which is capable to amplify at the specified bandwidth. An inverting configuration was chosen, because it only adds the offset voltage to the signal instead of adding it 33-fold in the case of a noninverting amplifier. A capacitor is added into the feedback of the second amplifier to match its bandwidth with the TIAs. This reduces overall RMS-noise by cutting off high frequency components of the Nyquist-noise, which has constant noise density. The implemented filter is equivalent to a Butterworth 1st order filter, but it may be sensibel to use higher order filters to improve noise rejection.

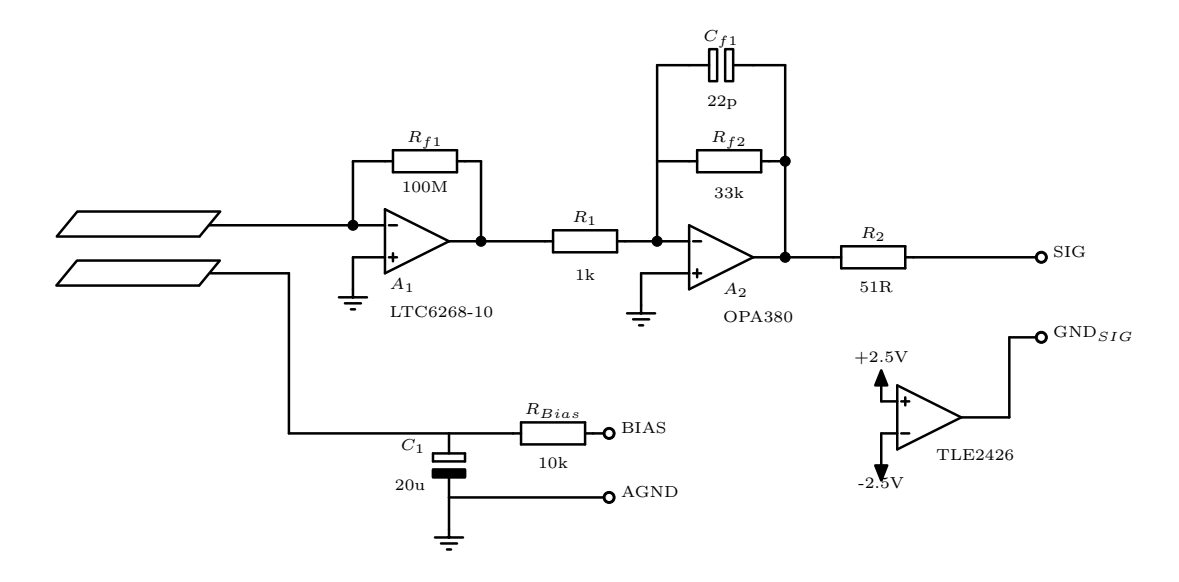


Figure 2: Simplified schematic of the amplifier. Shown is the TIA A_1 , the second inverting amplifier A_2 and the Rail Splitter TLE2426 which drives the Output GND_{SIG}.

2.3.2 Power Supply and Ground

Because this circuit should be able to perform in a vaccuum chamber and electrical feedthroughs are a scarce resource, as few external electrical connections as possible will be used. The operating voltage is therefore supplied in a single supply configuration and split into a symmetrical power supply on the circuit board. Great care was taken to minimize noise on this ground node, while at the same time achieving limited power dissipation, to avoid heating of the PCB in vacuum. Temperature gradients on the PCB could lead to thermoelectric voltages and affect the precision. Extensive simulations showed, that no active buffered ground voltage provided the same noise quality as a resistor voltage divider. A voltage divider however brings the problem of very limited current supply capability, because loading the voltage divider would change the ground node voltage. This is no problem for the two amplifiers, as both the TIA, as well as the inverting op amp only draw the input bias and input offset current from the ground node, which is in the pA range or below for the amplifiers used. The only substantial current from / to the ground node is the return current from the device (oscilloscope) attached to the output. A voltage divider, that can handle this load, without deviating to much would dissipate significant power. It was therefore decided to separate this ground node from the others. The return current is then fed to an active buffered ground voltage (GND_{SIG}) , just for the output, where the noise of this solution is acceptable due to the high signal levels. The TLE2426 "Rail Splitter Precision Virtual Ground" from Texas Instruments is chosen for this task. The remaining ground node connected to the non inverting inputs of the op amps is from now on referred to as AGND. The corresponding voltage divider is depicted in Figure 3.

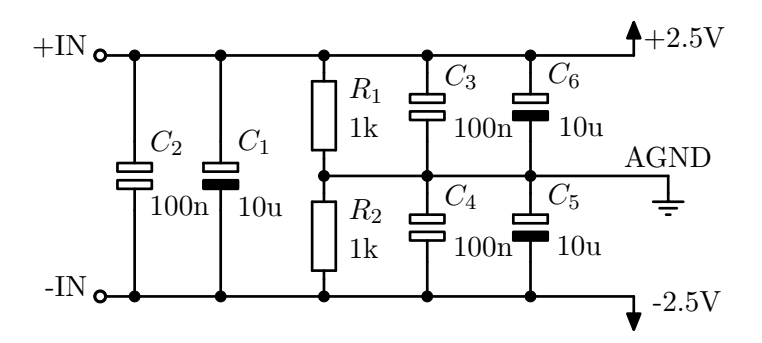


Figure 3: Schematic of the the network to achieve a low noise ground potential (AGND) at half supply voltage.

2.3.3 Temperature Control

A NTC is placed on the board close to the amplifiers in order to monitor the temperature of the PCB in a vaccuum environment. Its resistance is compared to four set values using comparators which drive LEDs with their outputs. This gives visual warning of temperature rise above four set temperatures (30°C, 35°C, 45°, 60°C).

2.3.4 PCB Layout

Careful decisions have been made considering the layout of the PCB in order to control parasitic properties and electromagnetic interference (EMI). To decrease parasitic currents to the input node, the silkscreen is not applied in this area, because it does not posses a specific resistance as high as the base material (FR-4). Additionally, a guard trace at AGND potential is used to "suck up" all currents from nearby traces, before they can reach the input node. Where the guard trace would unnecessary enlarge the capacitance visible to the input node, a slot has been milled into the PCB instead, as is visible in Figure 4.

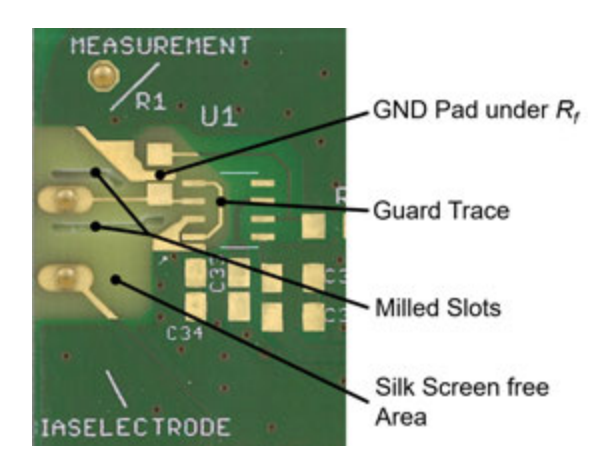


Figure 4: Input side of the amplifier PCB. The green silkscreen is removed around the input nodes and a guard trace is employed to prevent current leakage from surrounding traces on the right side.

The parasitic capacitance C_f of the feedback resistor R_f is limiting the bandwidth of the TIA and is therefore minimized. It can not be zero, however the minimum value to achieve stability, according to Equation 4, is so low, so that parasitic capacitance will always be greater and it therefore does not have to be considered. The maximum value to achieve stability is $0.1 \cdot C_{IN}$. Because C_{IN} is at least 0.5 pF, which is the differential input capacitance +1/2 common-mode-capacitance of the LTC6268-10 all $C_f < 50$ fF fulfill this requirement [12].

$$C_f > \sqrt{\frac{C_{IN}}{GBW \cdot R_f}} [12] \tag{4}$$

 C_f is minimized by using a physically large resistor (1206) and putting an AGND copper pour between its pads to shunt the electric Field to AGND, as visualized in Figure 5. [12]

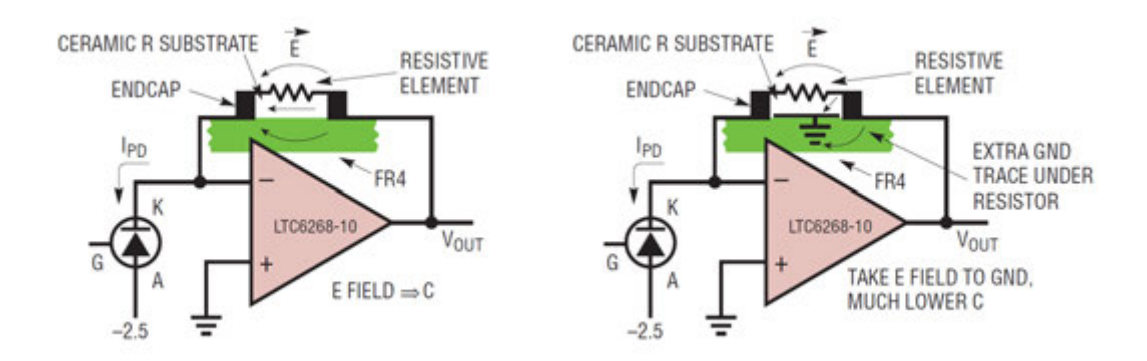


Figure 5: The feedback capacitance can be reduced by shunting the E-field across the resistor to GND. Image source: Linear Technologies [12]

To minimize the effect of incoming EMI noise, a multilayer structure is used with a solid internal AGND-plane and copper pours on the top plane, which are connected via heavy stitching. While the bottom plane is left intentionally unpopulated to allow mounting of a heat sink, it is used to connect traces in such a way, that all loop areas are as small as possible. As a final measure to further reduce EMI, a shield made of copper foil is placed above the amplifier section of the PCB and connected to AGND at several points.

2.3.5 Further Improvements

In hindsight, the approach to calculations in the design phase was naive, as the signal intensity of the measured pulses can not simply be compared to a DC current measurement. SNR improves with $\sqrt{R_f}$ for DC signals. However, this experiment aims to measure ultrafast pulses, with a duration so small that they can be approximated as delta peaks from the standpoint of an electronic (slow) amplifier. This means that there is a flat distribution of the signal in frequency space. Therefore the signal strength is proportional to the bandwidth of the amplifier. Because of this and the fact that the bandwidth is inversely proportional to the gain R_f , the signal amplitude should stay the same, regardless of what value is used for R_f , because the increased signal from added bandwidth is compensated by loss of gain. SNR is then proportional to $\frac{1}{\sqrt{R_f}}$, because the noise level is still Nyquist-noise. Applying this method to increase SNR would have the added benefit of shorter signal pulses at the output, thus enabling measurements at higher repetition rates.

There are limits to this, because the maximum bandwidth is limited by the op amps GBW and stability conditions. Another limit is set by the sharpness of the measured pulse, which may approximate a delta peak well enough in its optical form, but will be elongated by capacitance and inductance of the electrodes and input, as well as by flight times of the ions / electrons.

2.4 Verification

Different approaches are used to generate small currents to test the amplifier. An obvious method to generate small currents is to use large value resistors connected to a signal generator. The biggest low noise metal foil resistor easily obtainable is one with $68 \text{ M}\Omega(\text{VR}68000006805\text{JAC}00 \text{ from Vishay})$. In conjunction with a 500:1 voltage divider, this results in approximately 30 pA per V according to Ohm's law. While this is suitable to measure the gain at DC and low frequency, it is found that the parasitic capacitance of the resistor is limiting the precision of this method at higher frequencies, due to the extra current flowing. This effect is already substantial at 1 kHz. To mitigate this problem, a resistor with lower parasitics is chosen. The 100 M Ω \pm 1 % SMD resistor, which is also utilized in the amplifier itself, is used in combination with a -60 dB signal attenuator. The measurement of peak-to-peak amplitude results in a DC transimpedance of (3.38 ± 0.10) G Ω . All measured values are found in Table 1 and the calculated gain values are plotted in Figure 7. Although the influence of parasitic properties is reduced in the new setup, when measuring a square wave current, a settling time of 30 µs is observed. From this, one can conclude that for frequencies higher than the inverse of double the settling time (16 kHz) the current signal is significantly disturbed by the parasitic properties of the resistor and therefore the computed gain value is not accurate.

Table 1: Result of measurements with sinusoidal voltage U_{in} applied to TIA input via a 100 M Ω resistor. For different frequencies f the amplitude of the output voltage U_{out} is measured.

	1 0			· · · · · · · · · · · · · · · · · · ·	
f / Hz	Δf / Hz	U_{in} / mV	$\Delta U_{in} / \text{mV}$	U_{out} / mV	ΔU_{out} / mV
1.00	0.01	21.8	0.2	736	8
10.10	0.05	22.2	0.2	736	8
98.35	0.05	22.2	0.2	740	8
514.6	0.2	22.2	0.2	736	8
5174.0	0.2	22.4	0.2	746	8
25 828.0	0.5	23.0	0.2	916	8
33 726.5	0.5	23.2	0.2	1020	10
45 729	1	23.2	0.2	1030	10
59 439	1	23.6	0.2	1030	10
200 438	5	24.5	0.2	708	8
333 333	20	27	0.2	508	8
623 130	50	34.1	0.2	308	8
1 003 250	100	44.4	0.2	210	8

The approach of Bergsten et al. [1] is used to measure the gain at higher frequencies. A 10 pF capacitor is connected to the TIA input, which gives the following relation between applied voltage and current for a sinusoidal waveform:

$$I(t) = C \cdot \frac{dU_0 \sin \omega t}{dt} = C \cdot U_0 \cdot \omega \cos \omega t \tag{5}$$

$$I_0 = C \cdot U_0 \cdot \omega \tag{6}$$

The drawback of this method is the high uncertainty of the capacitor value of 10% and the frequency dependence of the current. Therefore very low frequencies can not be measured. The input voltage U_0 has to be adjusted for every frequency in order to stay in the input range of the TIA. Measurements are taken as peak-to-peak values to neglect offset voltage.

Table 2: Result of measurements with sinusoidal voltage U_{in} applied to TIA input via a 10 pF
capacitor. For different frequencies f the amplitude of the output voltage U_{out} is measured.

f / kHz	Δf / kHz	U_{in} / mV	ΔU_{in} / mV	U_{out} / V	ΔU_{out} / V
0.00104	0.00001	3280	20	0.7	0.02
0.01054	0.000002	384	4	0.9	0.02
0.10155	0.00004	69	1	1.54	0.02
0.9873	0.0005	16.6	0.1	3.64	0.02
9.96	0.001	1.55	0.01	3.27	0.01
22.966	0.001	0.71	0.01	3.08	0.04
31.502	0.001	0.65	0.01	3.1	0.02
42.189	0.001	0.65	0.01	3.34	0.02
57.482	0.001	0.65	0.01	3.44	0.02
104.84	0.03	0.68	0.01	3.52	0.04
308.6	0.03	0.72	0.06	2.5	0.4

Both methods assume that the input node of the TIA is at a AGND potential. This is reasonable, as long as the TIA is operated within its input range, because then the input node is a virtual ground which is only shifted by the offset voltage from the ground potential, applied to the non inverting input. As long as the voltage used to create the current, either at the capacitor or the resistor, is much greater than the offset voltage (typ. 0.2 mV according to [12]), all used formulas are a reasonable approximation.

The following method does not measure the actual gain of the TIA, but still provides information about the frequency response of the amplifier. In the experimental setup described below, laser pulses with a duration of only some fs are used to create a current pulse, fed to the TIA. Because the incoming current pulses are so short, they have a nearly constant power distribution in frequency space.

The outgoing signal from the TIA (as shown in Figure 6) is not as short any more, because the TIA attenuates the high frequencies. Fourier transforming the outgoing pulse shows this attenuation and therefore gives a good approximation of the frequency response. Because the current generated in the setup is unknown, the obtained frequency response gives only relative information. It is therefore normalized to the expected DC gain of 3.3 G Ω , in order to compare it to the capacitor and resistor based gain measurements in Figure 7. Both capacitor based measurement and Fourier transform show a corner frequency f_{-3dB} of about 34 kHz.

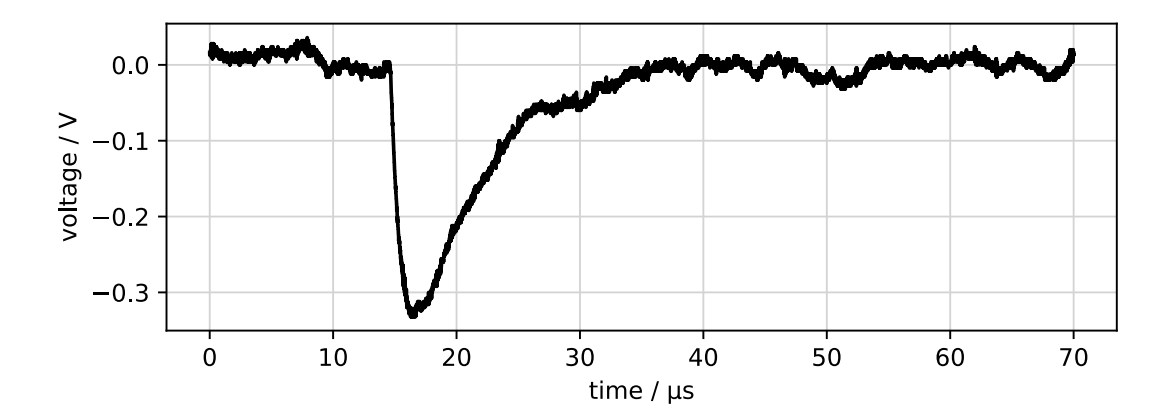


Figure 6: Output voltage U of the TIA over time t for the current created by a single laser pulse.

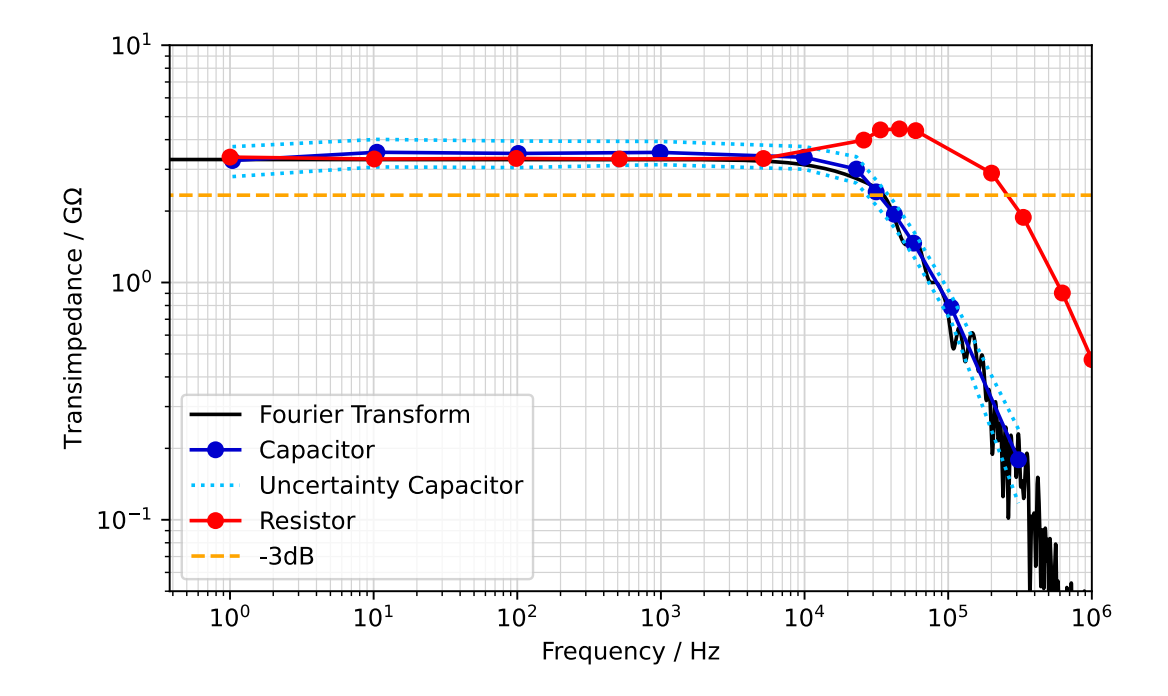


Figure 7: Transimpedance calculated from values of resistor (red) and capacitor (blue) based measurement in Table 1 and Table 2, plotted over frequency. The uncertainty of the resistor based measurement is constant at 3 %, however values above 16 kHz are not valid. The frequency response generated by Fourier transformation of a single pulse (Figure 6) is plotted in black. The Fourier transforms DC value is normalized to the expected 3.3 G Ω transimpedance, the orange dotted line is -3dB below that.

3 Experimental Setup

3.1 Electrical Setup

The described circuit is placed inside a shielding box with holes for the laser beam to pass through as shown in Figure 8. The box is connected to the negative supply rail. Two copper electrodes, each 8 by 15 mm big are attached to the input and bias points on the PCB of the TIA circuit, with a vertical distance of 9 mm \pm 1 mm. Power is supplied by a 9 V battery, with a linear 5 V regulator (LM7805), via a coaxial cable. The output is connected to an oscilloscope, which provides earth potential to the circuits GND_{SIG} and the bias input is shorted, unless noted otherwise. The box is then mounted on the optical table, utilizing PVC stand-offs in order to electrically isolate it. This photocurrent sampling box, from now on just referred to as "the box", is used to take measurements on a high intensity femtosecond laser in air.

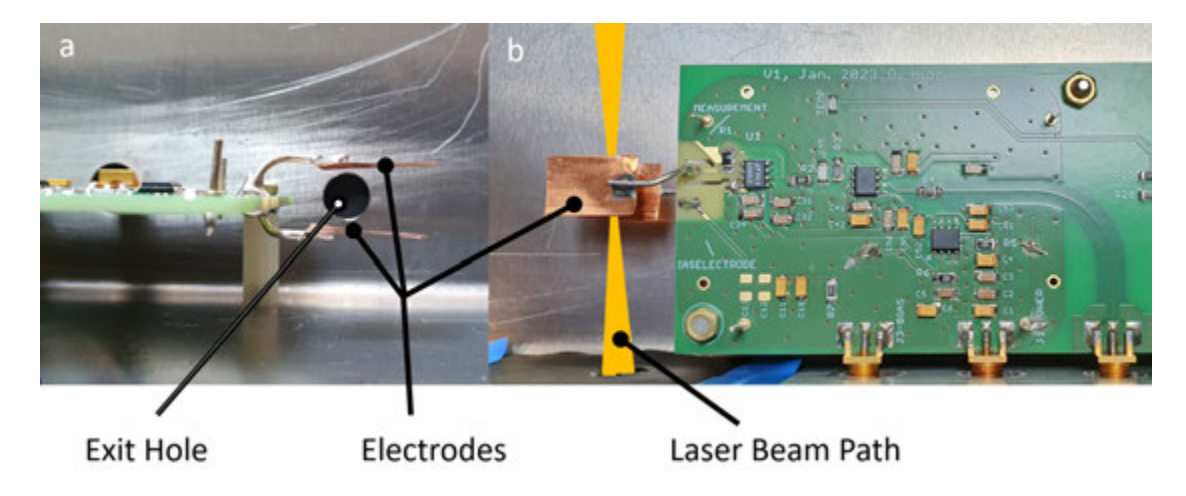


Figure 8: a: View through the entrance hole into the box, showing the electrodes that are attached to the PCB. b: Top view into the box, showing an illustration of the laser beam.

3.2 Optical Setup

The laser is taken from an existing experiment of Zhenhao Wang and diverted into the box. This existing setup spectrally broadens a pulse from an amplified Ti:sapphire Laser. The Laser has a repetition rate of 3 kHz and is not carrier envelope phase (CEP) stable. The broadening takes place inside a fibre, filled with neon gas, which can be seen on the bottom left of Figure 9.

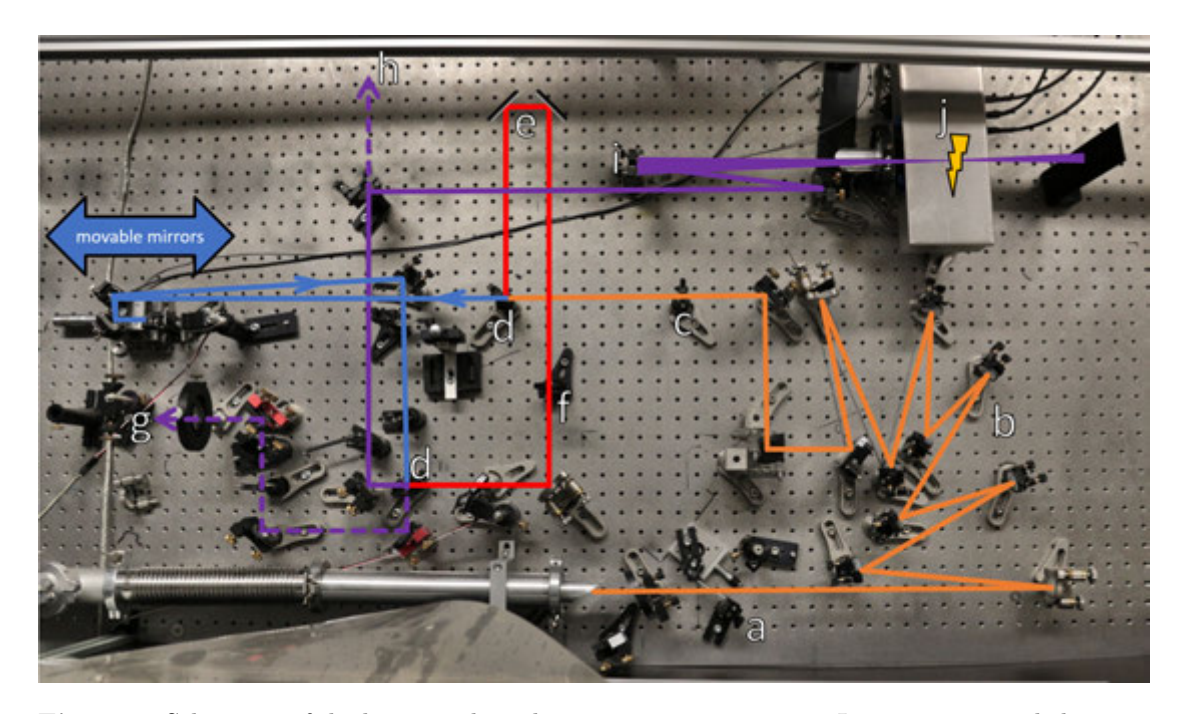


Figure 9: Schematic of the beam path in the time trace experiment. Important optical elements are labelled. The beam is entering the experiment from the silver tube on the left bottom, which contains the neon filled fibre. a) wedges to add normal dispersion b) chirped mirrors to add anomalous dispersion c) iris d) 50/50 beam splitter e) fixed mirrors. The real mirrors are positioned further away f) iris for red path g) beam path to spectrometer h) beam path to camera i) concave mirror, f = 40 cm j) Photocurrent sampling box. The electrodes inside are placed above and below the focal point.

In order to temporally compress this pulse, chirped mirrors (b) and fused silica wedges (a) create the appropriate amount of dispersion in the beam path. The so prepared pulses are sent into an Mach–Zehnder interferometer setup. The beam is separated into two at the first beam splitter (d) from where one part goes into the fixed length arm (e) and the other into the arm with movable mirrors. Those can be positioned on a course scale by means of a micrometer screw to have equal length in both arms. Movement on wavelength scale can be performed by a computer controlled piezo stage. Both beams are then merged again at the second beam splitter. One of the exiting beams is diverted to the spectrometer (g), while the other one is sent to the box (j). To reach the intensity necessary for nonlinear interaction, the beam is focussed by a concave mirror (i, f = 40 cm), with the focal point between the electrodes of the TIA. The beam then passes through the box and is stopped by a beamblock. To facilitate alignment of the two beams, the beam can also be diverted to the camera (h) by folding down a mirror.

3.3 Measuring a Single Pulse

After aligning the two beams to spatially overlap the temporal overlap was adjusted by changing the interferometers arm length until the spectrum of the recombined laser beam showed ripples. At this point the first current measurements can be taken. The output of the TIA is therefore attached to an oscilloscope which triggers on the lasers synchronization pulse. A pulse similar to Figure 6 can be observed, but the intensity varies with the electrode position. When the beam touches the electrode, the sign of the measured pulse is positive, otherwise negative. Marginal gains in amplitude can be achieved by positioning the beam close to a electrode, but ultimately the beam is positioned in the center between both electrodes, because this minimizes the sensitivity to small position fluctuations. By observing the amplitude of the pulse and utilizing the piezo stage for fine movement of the interferometers mirrors, the temporal overlap can be further adjusted until maximum signal amplitude is reached. In this position the fused silica wedges are brought into the beam path to compensate for chirp with additional dispersion in order to achieve a good temporal compression of the pulse. Because the maximum of amplitude could not be reached by fully inserting the wedges at first, another glass plate has been added to the beam path. With this additional dispersion a plateau of maximum signal intensity is found within the adjusting range of the wedges. Strong signals of multiple 100 mV are observed. Although they are above the noise floor, the signals still profit from averaging over multiple pulses. Such a measurement of 1024 averaged pulses is shown in Figure 11. because of the repetition rate $f_{rep} = 3$ kHz this measurement takes only about one third of a second.

3.4 Time Trace Measurement

By moving the mirrors on the piezo stage through the point of equal interferometer arm length and beyond, measurements of different time delays between the two beams can be taken. Because of the way the beam is folded in the movable arm of the interferometer, the length of the beam path depicted in blue in Figure 9 is changed by four times the piezo stage movement. This results in a time delay of

$$\tau = \frac{4 \cdot \Delta d_{piezo}}{c} \tag{7}$$

with c being the speed of light and d_{piezo} the distance of the piezo stage to the position of equal length beam paths. By varying this time delay and taking current measurements along the way, a time trace can be constructed.

3.4.1 Signal Acquisition

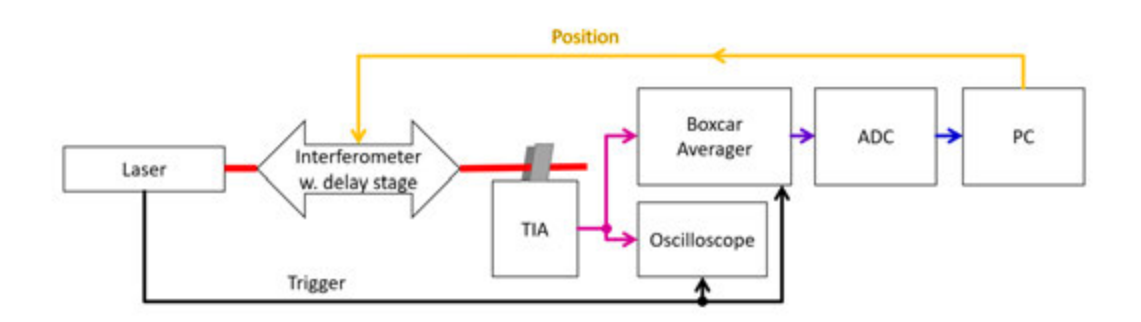


Figure 10: Block diagram of the time trace experiment. Focus is on the signal path, optics are omitted

In order to take reliable measurements, a method to determine the intensity of one pulse must be found. As shown in Figure 10, a boxcar averager is employed to reduce a pulse measured with the TIA to a single value. The analog output of the boxcar averager is then fed to a analog-to-digital converter (ADC) connected to a PC that stores the measurements and controls the piezo stage. The PC runs a program that reads the value from the ADC, then advances the piezo stage by a given step size and waits for it to settle. This cycle is repeated until the specified range is reached.

To tune the boxcar averagers parameters, a oscilloscope is also connected to the TIA output as well as to the gate signal of the boxcar averager. Both the instruments trigger on the same signal, provided by the laser just before each pulse. By displaying the gate of the signal over the signal from the TIA, a suitable delay and gate length can be set to include the main part of each pulse in the averaging. The parameters used are 1 µs delay and a gate width of 15 µs. It was found beneficial for the SNR to use the averaging of 30 individually triggered measurements, thus averaging for 10 ms at the given repetition rate of 3 kHz. This time is added to the waiting time of the program in order to only include measurements after the piezo stage has settled. Live monitoring of the TIAs signal facilitated by the oscilloscope also allows to adjust the laser intensity by closing the iris to a range where no saturation of the amplifier occurs.

3.4.2 Signal Distortion

A major source of distortion is the changing intensity of the laser beam, which varies on a time scale much shorter than what it takes to complete one time trace measurement. Those variations therefore are superimposed on the autocorrelation data. Because those variations are uncorrelated to the position of the delay stage, effects on the data could be mitigated by averaging many time traces. This however is not trivial, because the delay between both beams seems to be not perfectly reproducible. In the measurements shown in Figure 14 the highest peaks are aligned to compensate for offset between each

measurements.

4 Results

The resulting signal from a single Laser Pulse is shown in Figure 6. Averaging this signal over 1024 events results in the signal shown in Figure 11.



Figure 11: Output signal of the TIA (CH2) and Trigger signal from laser (CH1). This measurement shows the average of 1024 events.

Independent of the bias voltage applied to the lower electrode, a laser pulse creates a negative peak. This does not fit the prediction, as current into the TIA should give a positive signal on the output, because of the second inverting amplifier. Both electrons and positive ions are accelerated by the bias voltage in such a way that the technical current is directed into the TIA. One possible explanation is the effect of the housing which is at a negative voltage compared to AGND.

Because of the way the light path folds into the movable mirrors of the interferometer setup (see Figure 9), the change in optical distance is equal to four times the piezo stage movement Δd . Considering this and the speed of light, the displacement can also be viewed as a time delay τ between the two pulses.

$$\tau = \frac{4 \cdot \Delta d}{c} \tag{8}$$

The measurements will be presented on an axis converted to τ instead of the actually measured distance.

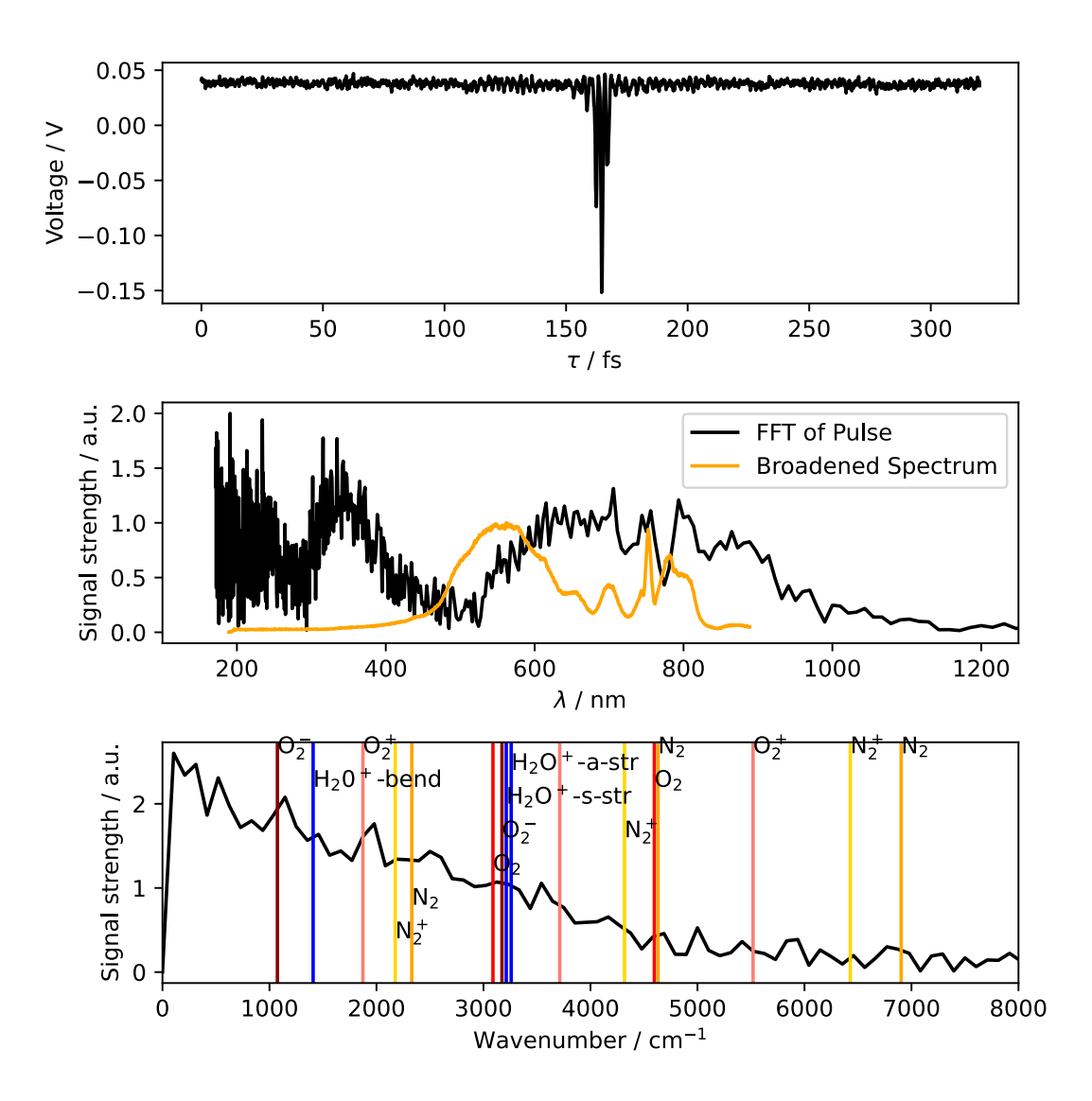


Figure 12: Time trace measurement of the laser pulse (top), its spectrum in the optical range (middle) and the infrared range (bottom). The optical spectrum is compared to a measured spectrum of the laser used in the experiment. Reference of different molecules vibrational levels are inserted in the infrared spectrum [6] [8] [11].

By Fourier transforming the timetrace, a spectrum can be obtained. The high frequency part of this spectrum is converted to a wavelength scale using a Jacobian conversion [9], in order to compare it to the measured spectrum of the broadened laser.

Although the Fourier transform of the timetrace in Figure 14 does not resemble the optical spectrum of the laser as a whole, features of the original spectrum are clearly visible between 650 and 750 nm. Due to the high order of nonlinearity, which is not compensated by any means in the present calculation, only the most intense parts of the laser pulse contribute to the autocorrelation.

By simulating the nonlinear autocorrelation of a cosine pulse with gaussian envelope, the order of the nonlinearity, as well as the pulse duration can be approximated. Depending on the order of nonlinearity, a FWHM (= $2.355~\sigma$) of 12 fs fits the measured data well. This is more than the 4 fs that the laser setup is capable of according to previous experiments. A probable cause is that the dispersion is not perfectly compensated, as only a plateau of maximum signal strength was used to adjust it instead of time series. According to the simulation, the order of nonlinearity seems to be in the range of 6 to 8, which overlaps with the predicted nonlinearity of multi-photon ionization of order 7 to 10 computed in the next chapter.

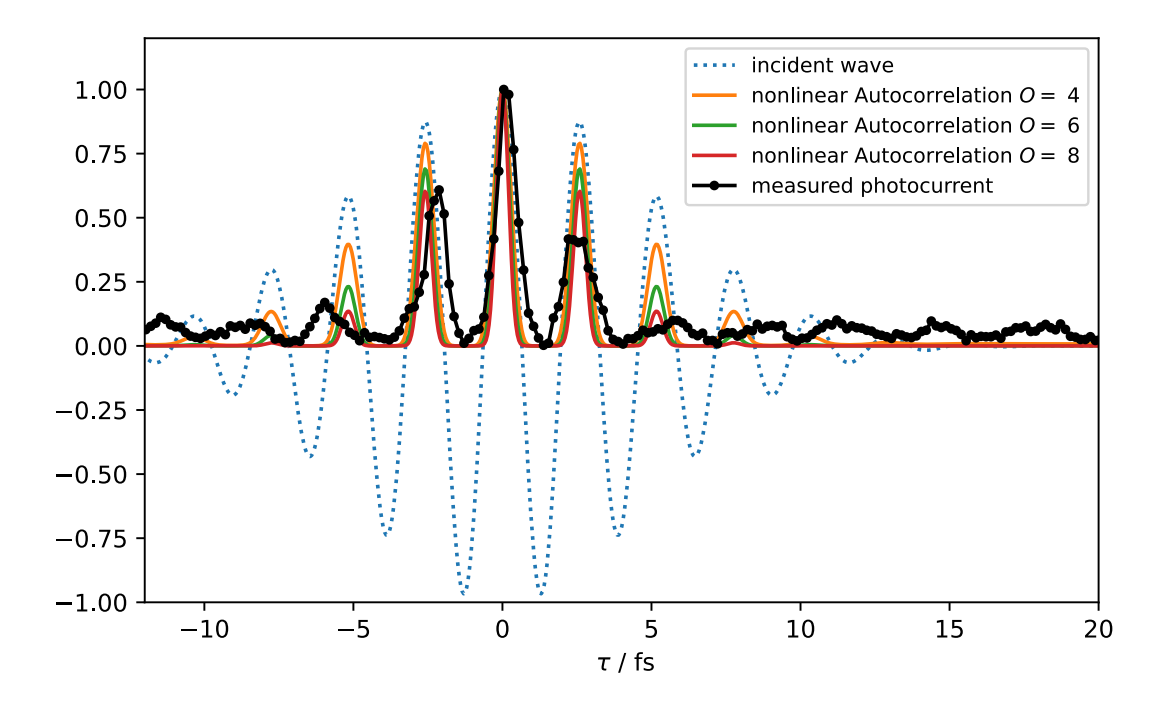


Figure 13: Simulation of nonlinear autocorrelation of a cosine pulse with gaussian envelope, $\sigma = 5$ fs, $\lambda = 780$ nm compared to photocurrent timetrace. All signals are normalized to a maximum value of 1 and the E-field used for the simulation is also displayed.

The low frequency part of the timetrace Fourier transform is also depicted in Figure 12. It is expected to show peaks at the vibrational levels of the medium of nonlinear interaction as will be explained in the next chapter. In the present experiment, air was the medium ionized by the laser, therefore its main constituents N₂, O₂ and H₂O are expected to show in the spectrum. Reference values of the vibrational levels of those molecules [6] [8] [11] are inserted into Figure 12. Some of those levels correspond to peaks but not all of them. This could be due to selection rules prohibiting some excitations or they are not intense enough to be resolved. Generally, because of the weak SNR within the spectrum, those results can not be deemed conclusive. The spectrum also lacks energy resolution. Many vibrational levels are separated by less wavenumbers

than the data points and could therefore not be resolved even with better SNR.

In an attempt to improve SNR multiple timetraces were taken without alterations to the experimental setup in order to average them. The individual measurements and the average are shown in Figure 14. Because the center of the tallest peak was shifted on each measurement, the individual measurements are shifted to compensate before averaging. This does not compensate drift within each measurement, thus the correlation between the measurements degrades with distance to the central peak, due to accumulated phase shift. It may also be the case that the carrier envelope phase changes, which would also induce a shift in the peak position. However, this will not be properly compensated by aligning tallest peaks.

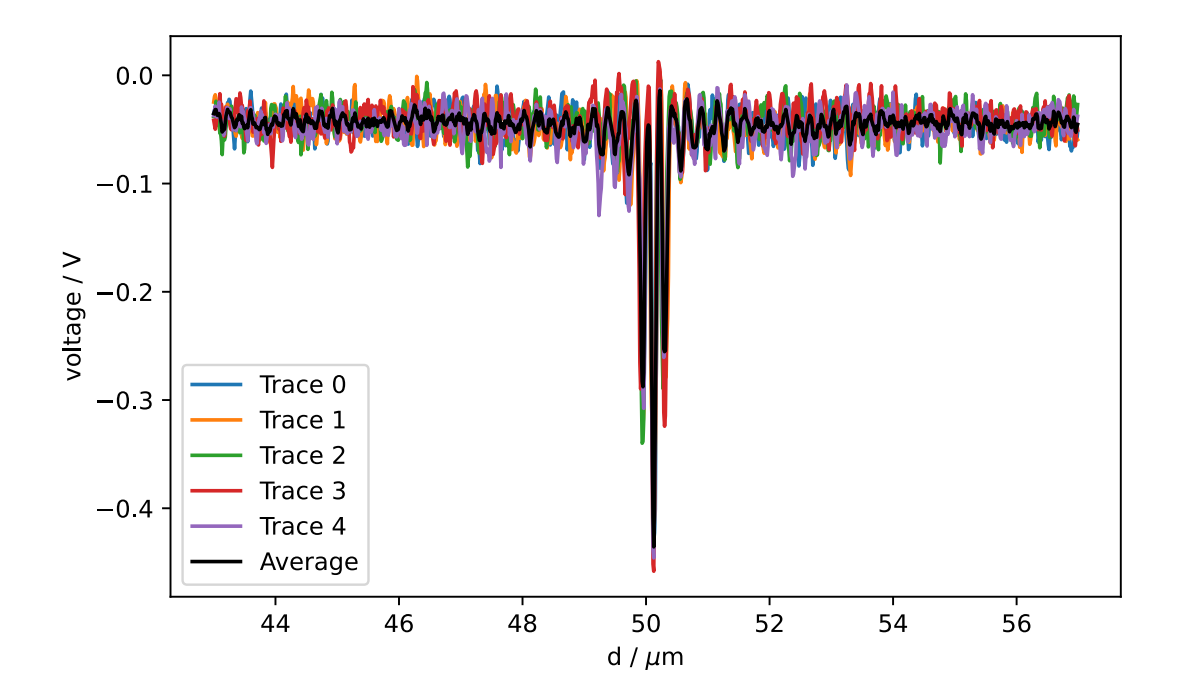


Figure 14: Time trace measurements of the laser pulse. Depicted is the measured voltage over the position d of the piezo stage and the average. All five traces are offset to align on their strongest peak.

5 Discussion

To analyze the observed time trace it will be split in two parts. The central region is dominated by non-sequential ionization, while the tails contain signals stemming from longer lived excitations, hence called sequential ionization. Non-sequential ionization can be described as a nonlinear process, either multiphoton ionization or tunnel ionization due to the lasers electrical field, described by the strong field approximation (SFA) [2]. This central region of the timetrace is essentially a nonlinear autocorrelation and can be used to gather information about pulse duration and its spectrum. In Figure 12 it can

be seen that some features of the optical spectrum of the laser can be reproduced by Fourier transforming the autocorrelation.

In a multi photon ionization process, the ionization rate is proportional to I^N , where I is the laser intensity and N the minimal number of photons required to reach the threshold energy. This proportionality is valid in the perturbative regime, however in the strong field regime $I > 10^{13} \ \mathrm{W \, cm^{-2}}$, where the experiment is conducted, this proportionality will decrease to approximately I^{N-1} [4]. The main constituents of air, N_2 and N_2 and N_2 have ionization energies of 15.581 eV \pm 0.008 eV and 12.0697 eV \pm 0.0002 eV respectively [8]. Assuming a photon energy of 1.59 eV corresponding to the center wavelength of the laser, this gives $N_{N_2} = 10$, $N_{N_2} = 8$, corresponding to a nonlinearity of order 7 to 10, depending on the laser intensity and on what molecules are ionized. This information can be used to retrieve the pulse length from the time series measurement as shown in Figure 13. To further improve this measurement, the laser intensity could be modulated while measuring the photocurrent. A power function fit of the resulting data would reveal the order of nonlinearity more precisely.

Sequential ionization (the tails of the timetrace) can be used to gather information about the intermediate states of the molecule under investigation. Because the experiment was conducted in air, mostly N_2 , O_2 and traces of H_2O are expected to interact with the laser pulse. Vibrational states can be excited by the first pulse and the second pulse provides the remaining energy to ionize the molecule. If an eigenstate of the molecule is excited by the first pulse, there will be no time evolution and the probability for ionization by the second pulse does not depend on τ . However if a superposition of states, with different vibrational quantum number ν , is excited as depicted in Equation 10, a beating of the wave function occurs due to the different eigenenergies E_{ν} of the eigenstates $|\psi_{\nu}\rangle$. In the quantum mechanic harmonic oscillator, the eigenenergies are:

$$E_{\nu} = \hbar \omega_e (\nu + \frac{1}{2}) \tag{9}$$

$$|\psi_o\rangle = c_a e^{\frac{-iE_a t}{\hbar}} |\psi_a\rangle + c_b e^{\frac{-iE_b t}{\hbar}} |\psi_b\rangle$$
 (10)

The beating occurs at the difference of the eigenfrequencies of the two states and is therefore:

$$f_{beat} = \frac{\Delta E_{a,b}}{h} = \frac{\omega_e}{2\pi} \cdot \Delta \nu_{a,b}$$

Due to this beating, the overlap of the excited wave function with the wave function of an ionized state is periodically changing.

$$\langle \psi_o | \psi_{ion} \rangle = \int \psi_o \cdot \psi_{ion} dx^3$$
 (11)

According to the Frank-Condon principle, the probability to excite from one state to another via dipole interaction is proportional to the overlap.

It is plausible that the beating of the nuclei wave function also affects the electronic

states and thus the following expression is modulated with the beating frequency:

$$\langle \Psi_{el,o} | \mathbf{r} | \Psi_{el,ion} \rangle$$
 (12)

This expression gives the interaction strength of the transition from $\langle \Psi_{el,o}|$ (the initial electronic state) to $|\Psi_{el,ion}\rangle$ (the electronic state after ionization) with photons, by evaluating the dipole operator \mathbf{r} .

By applying the Born-Oppenheimer approximation, this probability factorizes with the Franck-Condon factor of the much slower moving nuclei and the result is still modulated with the beating frequency. Hence the interaction with the second laser pulse is modulated with respect to delay time τ . We observe this as modulation of the ionisation probability in the time trace with $\frac{\Delta E_{a,b}}{h}$, which are the frequencies of the vibrational transitions of the molecule. By Fourier transforming the time trace, those modulations should show up at the characteristic frequencies.

In the above representation, other factors and quantum selection rules have been omitted and therefore not all transitions with finite probability will actually be allowed.

6 Conclusion

A new high bandwidth transimpedance amplifier for photocurrent sampling is designed, manufactured and tested. The circuit uses an LTC6268-10 operational amplifier in a 100 M Ω TIA configuration as input stage and an inverting amplifier as second stage. A transimpedance of 3.3 G Ω is achieved up to a corner frequency of 34 kHz. It is found to be a viable instrument for capturing nonlinear autocorrelation measurements of high intensity laser pulses in air. The possibility to probe the medium of nonlinear interaction for vibrational levels is explored, but more precise measurements are necessary to get conclusive results.

References

- [1] Tobias Bergsten, Karl-Erik Rydler, Ove Gunnarsson, Gunnar Eklund, and Valter Tarasso. A novel precision dc current source in the pa range. In *CPEM 2010*, pages 123–124, 2010.
- [2] C. I. Blaga, F. Catoire, P. Colosimo, G. G. Paulus, H. G. Muller, P. Agostini, and L. F. DiMauro. Strong-field photoionization revisited. *Nature Physics*, 5(5):335–338, 2009.
- [3] InterFET Corporation. 2N4117-8-9A. InterFET Corporation, March 2020.
- [4] Z. Deng and J. H. Eberly. Multiphoton absorption above ionization threshold by atoms in strong laser fields. *J. Opt. Soc. Am. B*, 2(3):486–493, Mar 1985.
- [5] Texas Instruments. Transimpedance amplifier circuit SBOA268A. Texas Instruments, February 2018.
- [6] Karl K. Irikura. Experimental Vibrational Zero-Point Energies: Diatomic Molecules. Journal of Physical and Chemical Reference Data, 36(2):389–397, 04 2007.
- [7] David L. Jones. μCurrent[™] GOLD. https://www.eevblog.com/projects/ ucurrent/. Accessed: 2023-03-30.
- [8] Peter Linstrom. Nist chemistry webbook. https://doi.org/10.18434/T4D303, 2017. Accessed: 2023-05-11.
- [9] Jonathan Mooney and Patanjali Kambhampati. Get the basics right: Jacobian conversion of wavelength and energy scales for quantitative analysis of emission spectra. The Journal of Physical Chemistry Letters, 4(19):3316–3318, 2013.
- [10] H. Nyquist. Thermal agitation of electric charge in conductors. Phys. Rev., 32:110–113, Jul 1928.
- [11] National Institute of Standards and Technology. Computational chemistry comparison and benchmark database, experimental data. https://cccbdb.nist.gov/exp2x.asp. Accessed: 2023-05-04.
- [12] Linear Technology. 4GHz Ultra-Low Bias Current FET Input Op Amp. Linear Technology, April 2015.